

Investigation of the immediate environment of Pr^{3+} ions in amorphous and crystalline PrNi_5 by calorimetry and neutron scattering methods

P. A. Alekseev, J.-B. Suck,¹⁾ S. N. Ishmaev, V. N. Lazukov, V. G. Orlov, I. P. Sadikov, and M. N. Khlopkin

I. V. Kurchatov Institute of Atomic Energy, Moscow

(Submitted 6 December 1990)

Zh. Eksp. Teor. Fiz. **99**, 1369–1386 (April 1991)

The specific heat, neutron diffraction, and inelastic magnetic neutron scattering were investigated for amorphous and polycrystalline samples of the intermetallic compound PrNi_5 . Amorphous PrNi_5 ($\text{Pr}_{16.7}\text{Ni}_{83.3}$) displayed a magnetic component of the inelastic neutron scattering and of the temperature dependence of the specific heat. The spectrum of magnetic excitations of amorphous PrNi_5 differed qualitatively from the spectrum of a crystalline sample due to excitation of transitions between well-defined f -electron levels of the Pr^{3+} ion in the electric crystal field (ECF). The high sensitivity of the ECF effects to local disorder and neutron diffraction with a high spatial resolution were used to study the characteristic features of the structure of the amorphous state of the intermetallic PrNi_5 and the transition from the amorphous to the equilibrium crystalline state. The splitting of the ground multiplet of the rare-earth ion in the ECF, recorded at different stages of annealing of the original amorphous alloy of the $\text{Pr}_{16.7}\text{Ni}_{83.3}$ composition, was deduced from the inelastic magnetic neutron scattering and specific heat measurements in magnetic fields up to 80 kG. The change in the local environment of the Pr^{3+} ion on transition from the amorphous (relaxed) to the crystalline state was quite abrupt. A comparison of the results obtained with the calculations based on a clear model of a deformed crystal demonstrated that allowing for the distribution of the angular parameters (local symmetry breaking) in the description of the local structure of the amorphous phase is as important as allowing for the distribution of the interatomic distances.

I. INTRODUCTION

1. Formulation of the problem

The problem of the structure of amorphous solids is not yet fully solved in spite of major experimental efforts. The main experimental methods for the investigation of the structure are x-ray and neutron diffraction,¹ which yield the radial distribution function of the atoms. The most detailed information can be obtained by neutron diffraction with a high spatial resolution and isotopic contrast.² The orientational distribution in the coordination of the nearest-neighbor atoms can be found only indirectly, by comparing the radial distribution functions of atoms using various models, and as a rule such information is tentative. A method sensitive to the angular distributions is needed in order to go beyond the information on the distribution of the atomic density averaged over the angles and determine the local topology of atoms, i.e., the real microscopic structure.

In principle, this can be done by investigating the splitting of the ground-state multiplet of a magnetic rare-earth ion in the electric crystal field (ECF) created by the immediate environment of this ion.³ A change in the angular distribution of ions, for example, in the transition from the axial to the equatorial distribution, alters the magnitude and sign of the coefficient B_2^0 which occurs in the ECF Hamiltonian and represents the gradient of a local electric field:

$$B_2^0 \propto \sum_j \frac{e^2 Z_j}{R_j^3} (3 \cos^2 \theta_j - 1). \quad (1)$$

On the other hand, if there are no changes in the distance between the atoms and in their number in the first coordination sphere, the radial distribution functions show

no changes. Interpretation of the results of an investigation of the properties of metallic glasses, which are sensitive to the quadratic component of the ECF (low-temperature thermodynamics,^{4,5} hyperfine and quadrupole splitting of the nuclear levels⁶), shows that there is a considerable difference between the local orientational order and that predicted, for example, by the model of random dense packing. It is found that the short-range order in substances of this kind is fairly specific and in some cases its influence on the measured characteristics differs little from the influence of the short-range order in a crystal.

The most effective spectroscopic method for the investigation of the ECF is inelastic magnetic neutron scattering. Transitions between the levels of the f -electron shell of a rare-earth ion, which appear because of lifting of the degeneracy of the J multiplet in the ECF, can be identified reliably in low-temperature experiments involving a small momentum transfer, when the contribution of phonons to the dynamic structure factor $S_d(\theta, \omega)$ is quite strongly suppressed.³ Important information on the structure of the lower f -electron levels and their wave functions can be obtained also by measuring the magnetic contribution to the temperature dependence of the specific heat in various magnetic fields.

Amorphous substances are thermodynamically unstable and undergo a transition to one or several crystalline phases at temperatures $T > T_{cr}$ where T_{cr} is the characteristic crystallization temperature. Studies of the characteristic features of this transition by inelastic magnetic neutron scattering provide very interesting results because of the high local sensitivity of the ECF effects.

The presence of structure in the spectrum of inelastic

magnetic neutron scattering in a sample of a metallic glass of the $(Y_{0.95}Er_{0.05})_{0.63}Cu_{0.37}$ composition was first demonstrated in Ref. 7. However, no comparisons with the crystalline analog and a quantitative analysis of the results were made.

We investigated the intermetallic compound $Pr_{16.7}Ni_{83.3}$ ($PrNi_5$), which was selected for the following reasons. Firstly, the reported diffraction investigations of the isostructural compound $LaNi_5$ (Ref. 8) led us to expect that the transition from the amorphous state to the thermodynamically stable hexagonal structure of the $CaCu_5$ type should occur without any intermediate phases. Secondly, the energy level scheme of the ECF levels of Pr^{3+} in crystalline $PrNi_5$ was known well.⁹ Our aim was to investigate the influence of the various stages of annealing of the initially amorphous $Pr_{16.7}Ni_{83.3}$ on the short-range atomic order by high-resolution neutron diffraction and inelastic magnetic neutron scattering. In addition, we measured the specific heat of amorphous and crystalline $PrNi_5$ samples and of the isostructural compound $LaNi_5$ in magnetic fields up to 80 kG in order to study the influence of amorphization on the density of states in the magnetic and phonon subsystems.

A combination of structural, spectroscopic, and thermodynamic methods allowed us to determine experimentally the nature of changes in the spectrum of states of the local magnetic moment. We then used the radial distribution function of atoms in model calculations in order to identify the topological characteristics of the short-range order in the amorphous state.

2. Experimental methods

The elastic structure factor $S(Q)$ determined in a diffraction experiment, is related to the reduced radial distribution function $G(r)$ of atoms by the Fourier transformation

$$G(r) = \frac{2}{\pi} \int_0^{Q_{max}} M(Q) Q [S(Q) - 1] \sin Q \, dQ, \quad (2)$$

where $M(Q)$ is the modification function.¹⁰ The upper limit of integration is related to the capabilities of the method and it in turn determines the accuracy of the function $G(r)$ obtained in this way.

If the "white" spectrum is combined with the time-of-flight technique employing a pulsed neutron source, this integration limit is 3–4 times higher than in the case of a conventional diffraction experiment, which naturally results in a higher precision of the determination of $G(r)$. The function $G(r)$ for an alloy or a compound is a weighted sum of the partial atomic distributions $G_{ij}(r)$ calculated allowing for the concentrations c_i and c_j of the alloy components and for their neutron amplitudes b_i and b_j :

$$G(r) = \sum_{ij} W_{ij} G_{ij}(r)$$

in the case of $Pr_{16.7}Ni_{83.3}$, the function in question is

$$G(r) = 0,848 G_{NiNi}(r) + 0,146 G_{NiPr}(r) + 0,006 G_{PrPr}(r) [W_{ij} = c_i c_j b_i b_j / (c_i b_i + c_j b_j)^2]. \quad (3)$$

It therefore follows that the main contribution to the radial distribution function of atoms in the alloy with $PrNi_5$ stoichiometry is made by the Ni–Ni and Ni–Pr distributions.

Inelastic magnetic scattering of thermal neutrons by the rare-earth paramagnetic ion in the investigated compound is thus governed mainly by the magnetic-dipole transitions between the various states of the total momentum of the ion that appear because of the splitting of the ground multiplet in the crystal field of the immediate environment.

The double differential scattering cross section is

$$\frac{d^2\sigma}{d\omega \, d\Omega} = \frac{k_f}{k_0} S_d(Q, \omega),$$

where k_f and k_0 are the momenta of the scattered (final state) and incident neutrons, $S_d(Q, \omega)$ is the dynamic structure factor obtained in the single-ion approximation:

$$S_d(Q, \omega) = \frac{1}{4} \left(\frac{1,91e^2}{m_e c^2} \right)^2 g_J^2 F^2(Q) \times \sum_{ij} |\langle i | J_{\perp} | j \rangle|^2 \rho_i(T) \delta(E_i - E_j - \hbar\omega), \quad (4)$$

and $\hbar\omega = E_0 - E_j$ is the change in the neutron energy. The first factor in the above expression determines the scale of the effect and it amounts to 0.29 b, $F(Q)$ is the magnetic-dipole form factor, whereas the matrix elements in the population factor

$$\rho_i(T) = \exp(-E_i/T) / \sum_k \exp(-E_k/T)$$

are related to the energy and the wave functions of the levels of the rare-earth ion, which can be calculated using the phenomenological ECF Hamiltonian:

$$\hat{\mathcal{H}}_{ECF} = \sum_{n,m} B_n^m \hat{O}_n^m. \quad (5)$$

In the case of the hexagonal symmetry of crystalline $PrNi_5$ the Hamiltonian $\hat{\mathcal{H}}_{ECF}$ contains just four terms:

$$\hat{\mathcal{H}}_{ECF} = B_2^0 \hat{O}_2^0 + B_4^0 \hat{O}_4^0 + B_6^0 \hat{O}_6^0 + B_6^6 \hat{O}_6^6 \quad (6)$$

(B_n^m are the phenomenological ECF parameters and \hat{O}_n^m are the equivalent operators) and the ground state 3H_4 of Pr^{3+} splits into three singlets and three doublets.

The relative positions of the levels and of the probabilities of the transitions between them are governed primarily by the configuration of the immediate environment formed by 18 nickel ions. The layer following nickel contains the rare-earth ions and makes a definite, but—as demonstrated experimentally in Ref. 11—a small contribution to the ECF potential.

Since the value of the double differential cross section of magnetic scattering involving transitions between the ECF levels is comparable with the phonon (nuclear) incoherent scattering, it is essential to study the temperature and momentum (angular) dependence of the scattering intensity in order to separate the magnetic and phonon contributions to the experimentally observed spectrum.

One of the thermodynamic characteristics most sensitive to the ECF effects is the magnetic component of the low-temperature specific heat.

This component is described by the expression

$$\Delta C_{CF} = -\frac{R}{T^2 Z} \left\{ \sum_i E_i^2 \exp\left(-\frac{E_i}{T}\right) - \frac{1}{Z} \left[\sum_i E_i \exp\left(-\frac{E_i}{T}\right) \right]^2 \right\}, \quad (7)$$

where

$$Z = \sum_i \exp(-E_i/T).$$

Although Eq. (7) does not contain explicitly [in contrast to $S_d(Q, \omega)$] the wave functions of the ECF levels but only their energies E_i , the use of an additional parameter in the form of a strong external magnetic field makes it possible to determine the nature of the wave functions. Fields of intensity in the 100 kG range completely lift the degeneracy of the multiplet and can alter considerably the level positions in accordance with the nature of the actual wave functions.

Important information on the scale of splitting, and on the nature of the ground state can be provided also by the temperature dependence of the entropy, defined as follows:

$$S(T_0) = \int_0^{T_0} \frac{C(T)}{T} dT. \quad (8)$$

An investigation of the temperature dependence of the magnetic contribution to the specific heat can give information on the nature of the spectrum of the localized moment and is particularly useful in providing information on the ECF splitting in the low-energy part of the spectrum ($\leq 4-5$ meV). Note that in order to distinguish the magnetic contribution, we have to determine the specific heat of both PrNi_5 and of the nonmagnetic structure analog of LaNi_5 under the same conditions.

II. EXPERIMENTS

1. Samples

Our amorphous intermetallic compound was prepared by the method of ion-plasma sputtering of a polycrystalline PrNi_5 target in an argon atmosphere by a technology similar to that used earlier to prepare amorphous LaNi_5 (Ref. 12). The amorphous structure of our sample was determined by x-ray and neutron diffraction. The stoichiometric composition was checked by x-ray fluorescence analysis and by x-ray phase analysis of annealed (crystallized) amorphous samples.

The different stages of annealing of the amorphous and crystalline states were identified by a heat treatment method, involving heating the sample in a vacuum of at least 10^{-5} torr at a constant rate selected in the range from 3 to 40 K/min up to a fixed temperature $T_{\max} \leq 1000$ K followed by rapid cooling at initial rates approximately an order of magnitude higher than the heating rate.

In this way we were able to ensure "freezing" of the state of structural relaxation reached in the course of heating. Annealing could be carried out under adiabatic and nonadiabatic conditions. This method was used to investigate the influence of the heating rate on the crystallization temperature T_{cr} of $\text{Pr}_{16.7}\text{Ni}_{83.3}$ samples, defined as the annealing temperature at which clear diffraction peaks were observed. It was found that the transition from the amor-

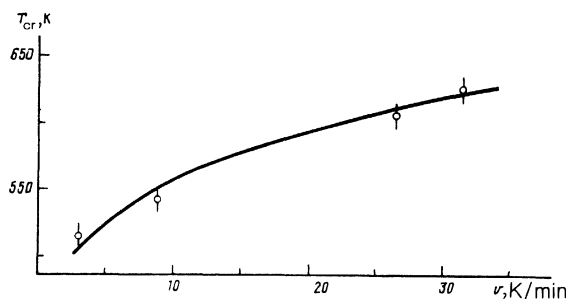


FIG. 1. Dependence of the crystallization temperature on the annealing rate v of amorphous $\text{Pr}_{16.7}\text{Ni}_{83.3}$. The points are the experimental values and the curve is calculated using a model¹³ with an activation energy $\Delta E = 450$ kJ/mol.

phous to the crystalline state occurred, within the limits of the experimental precision, directly to the thermodynamically stable phase of the CaCu_5 type, by analogy with LaNi_5 (Ref. 8). The dependence of the crystallization temperature (Fig. 1) on the heating rate agreed with the model of crystallization at growth nuclei.¹³

Our neutron experiments were carried out on a number of samples which reached different stages of annealing (their main properties are listed in Table I). Samples 1.1.1–1.1.2 and 1.2.1–1.2.3 were prepared from sample No. 1 by dividing it into two parts (1.1 and 1.2) and annealing. Samples Nos. 1, 2, and 3 were made from the same piece of the original amorphous material with the $\text{Pr}_{16.7}\text{Ni}_{83.3}$ composition.

We were able to prepare samples in states quite close to the point of crystallization from the amorphous or crystalline phases. The two highest temperatures of annealing of a sample in the amorphous state (samples 1.1.2 and 1.2.1) differed by less than 3% from the expected crystallization temperature. The difference between the annealing temperatures when the sample was still amorphous (531 K, sample 1.1.2) and already crystalline (543 K, sample 3) was also $\sim 3\%$ of the crystallization temperature. The original amorphous samples before annealing and all nine annealed samples were investigated using an IN-4 time-of-flight spectrometer using the high-flux reactor at the Laue-Langevin Institute.

Four samples (originally amorphous, annealed to 488 K, No. 3, and No. 1.2.3) were used to determine the structure factors employing a multidetector time-of-flight diffractometer in conjunction with the Fakel accelerator.

2. Results of measurements

a) Inelastic neutron scattering

Inelastic neutron scattering was determined in the range of transferred energies from +15 meV to –100 meV within the angular range from 4.2 to 75.6°. The energy of the incident neutrons E_0 was 17.8 meV and the full width at half-maximum (FWHM) of the elastic scattering line was 0.9 meV. These measurements were carried out at temperatures from 15 to 200 K.

The time-of-flight spectra and the results of calibration using a vanadium standard, together with measurements on empty and cadmium-shielded containers, were used to determine the dynamic structure factor $S_d(\theta, \omega)$, where θ is the scattering angle. The scattering functions $S_d(\theta, \omega)$ were

TABLE I.

Sample No.	T_0 , K	State	\bar{T}_{cr} , K***	v , K/min	m , g
1	479	A	523	4,5	15
1.1.1	500	A	523	4,5	7,8
1.1.2	531	A	540	6,0	6,4
1.2.1	521	A	530	5,0	7,1
1.2.2	571	C	530	5	6,8
1.2.3	1033 *	C	—	—	6,6
2	833	C	530	5	13
2.1	1053 **	C	—	—	13
3	543	C	515	4	3,8

Notation. Here, T_0 is the maximum temperature attained during annealing; \bar{T}_{cr} is the expected crystallization temperature; v is the annealing rate; n is the mass of the sample; A is amorphous and C is the crystalline sample.

*Annealing duration 70 min.

** Annealing duration 30 min.

***Values of \bar{T}_{cr} calculated using the model of Ref. 13 (see also Fig. 1).

determined for the crystallized samples (Fig. 2).

Two transitions from the ground state Γ_4 to Γ_{5A} at 4 meV and to Γ_3 at 13 meV (the inset in Fig. 2 gives the energy level scheme from Ref. 9), were responsible for two sharp peaks in the spectrum recorded at the lowest temperature 17 K used in our measurements. Since this temperature was comparable with the scale of splitting between the ground and nearest excited levels Γ_6 and Γ_1 , an analysis of the spectrum should allow for the contribution of the low-energy transitions between these levels to the scattering, which (because of insufficient resolution of the spectrometer) was manifested experimentally in the form of a shoulder near the base of the elastic peak. After the temperature was increased, a peak appeared near 8 meV, corresponding to the transition from the Γ_{5A} to the Γ_3 level. The background intensity between the peaks was clearly due to incoherent nuclear scattering.

The observed spectra of the transitions between the ECF levels of crystallized $\text{Pr}_{16.7}\text{Ni}_{83.3}$ could thus be completely described within the framework of the splitting

scheme established earlier for polycrystalline PrNi_5 in Ref. 9.

In contrast to the spectrum of a crystallized sample, we found no clear structure in the spectrum of the original amorphous $\text{Pr}_{16.7}\text{Ni}_{83.3}$ determined at temperatures in the range 15–200 K (Fig. 3). The value of $S_d(\theta, \omega)$ manifests a considerable increase in the scattering intensity in the limit $\hbar\omega \rightarrow 0$ (near the base of the elastic peak). The angular and temperature dependence demonstrated that the magnetic scattering contribution to $S_d(\theta, \omega)$ dominates. The low-temperature asymmetry of the spectrum relative to $\hbar\omega = 0$ was due to the influence of the population factor in Eq. (4) in accordance with the principle of detailed balance. An analysis of the ratio of the total intensities in the range $|\hbar\omega| \leq 3.5$ meV and $\hbar\omega > 3.5$ meV in the amorphous and crystalline states demonstrated redistribution of the scattering intensities as a result of amorphization in favor of the region near the elastic peak. It should be pointed out that all the heat-treated samples which remained in the amorphous state (Nos. 1.1.1, 1.1.2, 1.2.1) had $S_d(\theta, \omega)$ spectra similar to

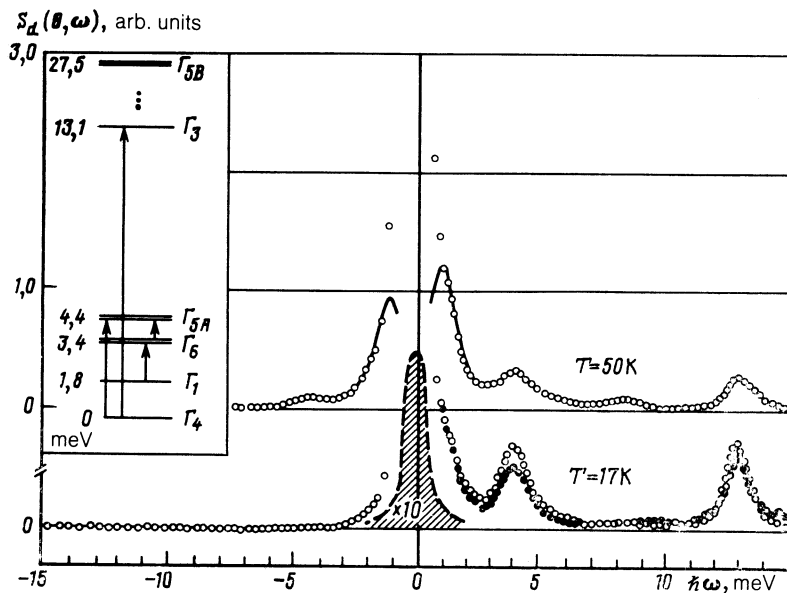


FIG. 2. Dependences $S_d(\theta, \omega)$ for sample No. 2 annealed up to 833 K; \circ $\langle \theta \rangle = 13^\circ$; \bullet $\langle \theta \rangle = 50^\circ$, $E_0 = 18$ meV, measurement time 200 min. The inset shows the energy level scheme in the ECF of PrNi_5 with the hexagonal symmetry;⁹ the transitions that may occur at $T = 17$ K are identified by arrows. The shaded peak corresponds to the elastic scattering of neutrons by the nuclei.

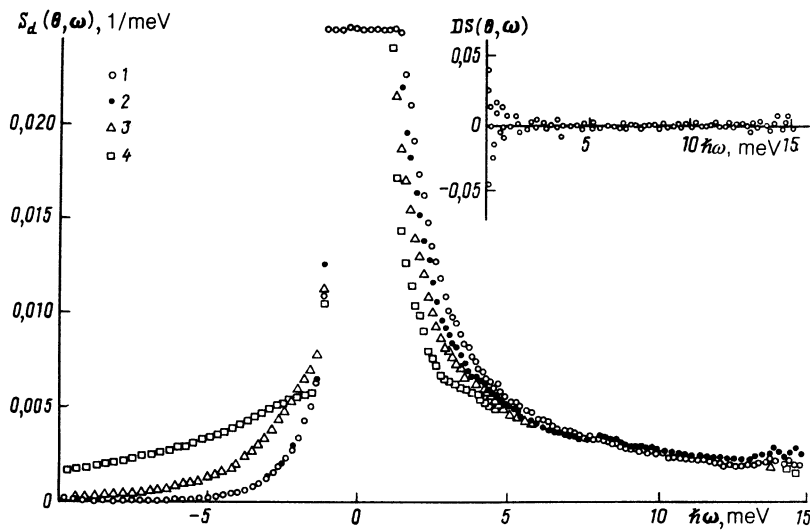


FIG. 3. Form of $S_d(\theta, \omega)$ obtained for the original amorphous sample of $\text{Pr}_{16.7}\text{Ni}_{83.3}$: 1) $\langle \theta \rangle = 13^\circ$, $T = 16$ K; 2) $\langle \theta \rangle = 59^\circ$, $T = 16$ K; 3) $\langle \theta \rangle = 13^\circ$, $T = 50$ K; 4) $\langle \theta \rangle = 13^\circ$, $T = 200$ K. The inset shows the difference $DS(\theta, \omega)$ between $S_d(\theta, \omega)$ for the original amorphous and the annealed sample No. 1.2.1.

those shown in Fig. 3. This quantitative similarity could be described by a difference $DS(\theta, \omega)$ between the spectra exhibited by samples which were annealed nearly to the crystallization temperature and the original amorphous samples, as demonstrated as the inset in Fig. 3.

On the other hand, all the crystallized samples had spectra similar to that shown in Fig. 2 for the thermodynamic equilibrium state. Definite quantitative differences were observed. Firstly, the widths of the peaks in the spectrum for a sample immediately after crystallization (No. 3) were somewhat greater (by 0.1–0.15 meV) than in the case of a sample in thermodynamic equilibrium; secondly, the positions of the peaks corresponding to the Γ_4 – $\Gamma_{5,4}$ and Γ_4 – Γ_3 transitions in sample No. 3 were shifted by 0.1–0.15 meV toward higher energies. This effect was manifested clearly in the difference spectrum shown in Fig. 4.

b. Specific heat in magnetic fields up to 80 kG

The specific heat of LaNi_5 and PrNi_5 samples was measured in magnetic fields of 0, 40, and 80 kG at temperatures in the range 1.5–50 K by an adiabatic method.¹⁴ Samples were thin plates and the magnetic field was directed at right-angles to the flat surface. The error in the determination of the specific heat was of order 3% in the case of amorphous samples and 0.7% in the case of crystalline samples.

In the investigated temperature range the specific heat

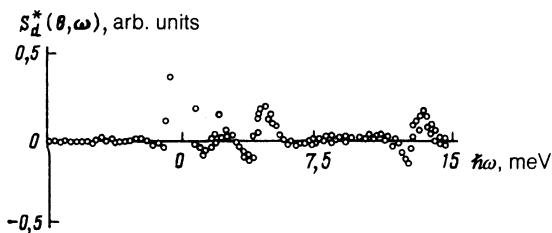


FIG. 4. Difference $S_d^*(\theta, \omega) = S_d(543 \text{ K}) - S_d(1033 \text{ K})$ for $\text{Pr}_{16.7}\text{Ni}_{83.3}$ samples annealed at 543 K and 1033 K.

of amorphous LaNi_5 was higher than that of crystalline material and at temperatures above 5 K the main contribution was made by the phonon subsystem. Figure 5 shows the temperature dependence of the ratio of the differences between the specific heats of the amorphous and crystalline LaNi_5 to the specific heat of crystalline LaNi_5 . A maximum was typical of the amorphous systems¹⁵ and indicated softening of the phonon spectrum as a result of the amorphization process.

The magnetic field had practically no influence on the specific heat of LaNi_5 . In the case of PrNi_5 a strong dependence of the specific heat on the magnetic field was observed in the crystalline and amorphous states. Assuming that the phonon spectrum and the density of the electron states at the Fermi level were the same in the lanthanum and praseodymium compounds, it was possible to use the difference between their specific heats to find the contribution ΔC_M due to the splitting of the ground state of the Pr^{3+} ion by the crystal field. The experimental results are shown in Fig. 6. In

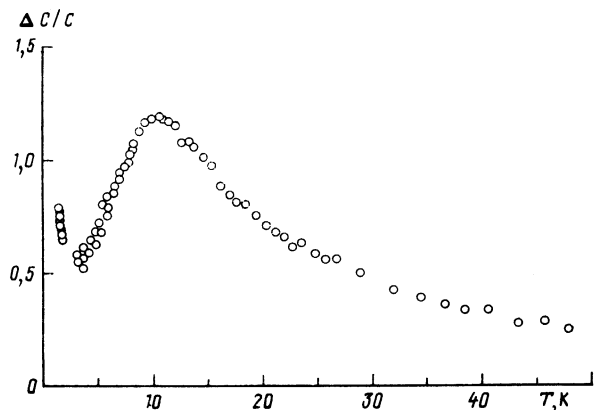


FIG. 5. Temperature dependence of the relative value of the difference between the specific heats of amorphous and crystalline LaNi_5 defined as $\Delta C/C = (C_{\text{am}} - C_{\text{cr}})/C_{\text{cr}}$.

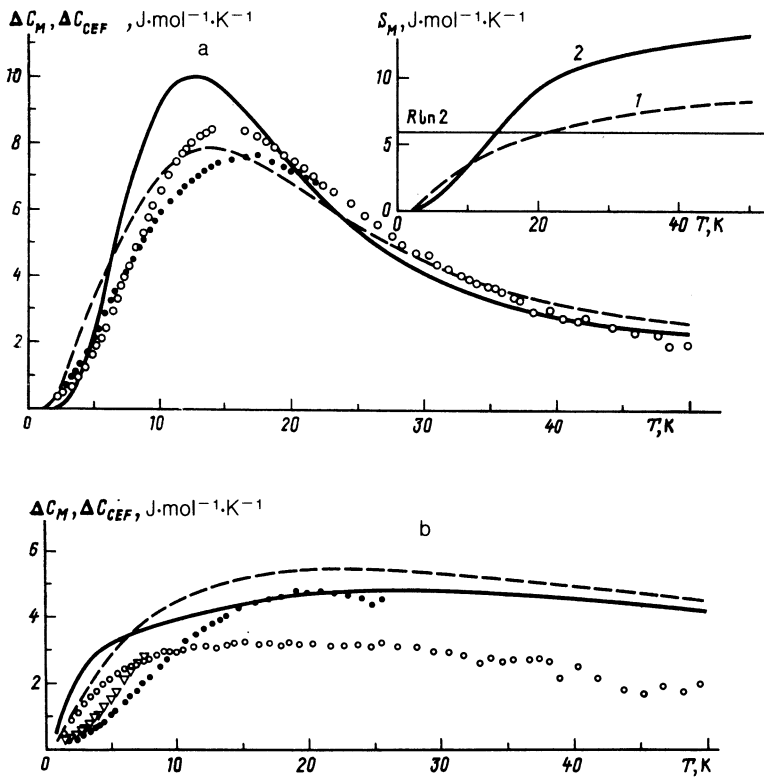


FIG. 6. Temperature dependence of the experimental (ΔC_M) and calculated (ΔC_{ECF}) magnetic contributions to the specific heat of amorphous and crystallized $\text{Pr}_{16.7}\text{Ni}_{83.3}$: a) crystallized sample; b) original amorphous sample; \circ) experiments in a field of 0 kG; \bullet) experiments in a field of 80 kG; ∇) experiments in a field of 40 kG; the continuous curves are calculated for 0 kG and the dashed lines for a field of 80 kG. The inset shows the experimentally determined magnetic contributions to the entropy of $\text{Pr}_{16.7}\text{Ni}_{83.3}$ samples in a zero magnetic field: 1) amorphous; 2) crystalline sample.

the amorphous and crystalline states the temperature dependence of ΔC_M passed through a maximum at a temperature of the order of 15 K, but the amplitude of the maximum in the amorphous state was considerably less and the maximum itself was broadened. In the case of crystalline PrNi_5 the application of a magnetic field led to a slight broadening and lowering of the maximum, and to a small shift in its position toward higher temperatures. On the other hand, the amplitude of the maximum of the amorphous PrNi_5 in-

creased by a factor of 1.5 in the magnetic field and the maximum itself became more pronounced.

It should be pointed out that the temperature dependence of ΔC_M obtained for the amorphous PrNi_5 at low temperatures ($T < 5$ K) was nearly linear in a zero magnetic field, but when the field was increased, it became nearly exponential. This exponential temperature dependence indicated the presence of a gap in the spectrum of elementary excitations, whereas the linear dependence corresponded to

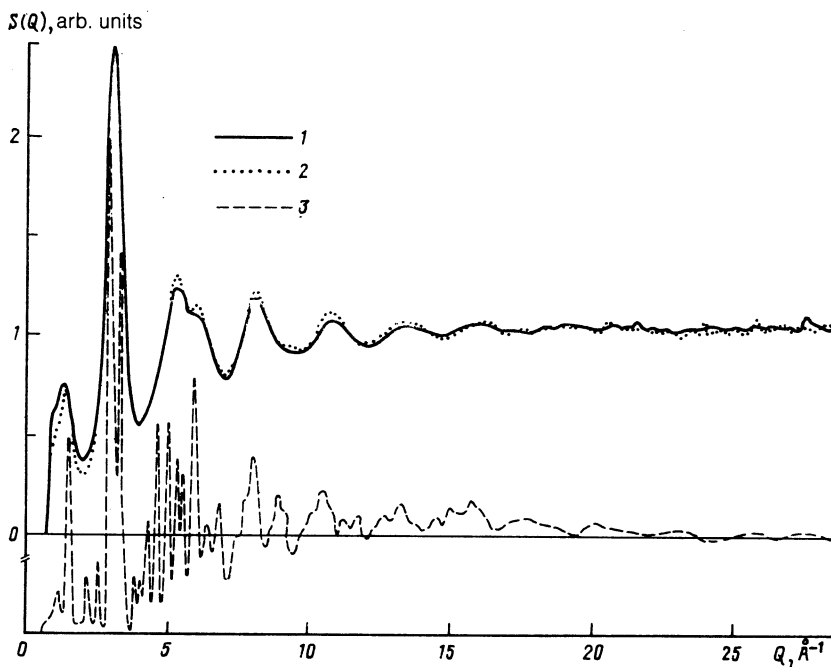


FIG. 7. Structure factors of amorphous (1), amorphous annealed (2), and crystalline (3) samples of PrNi_5 .

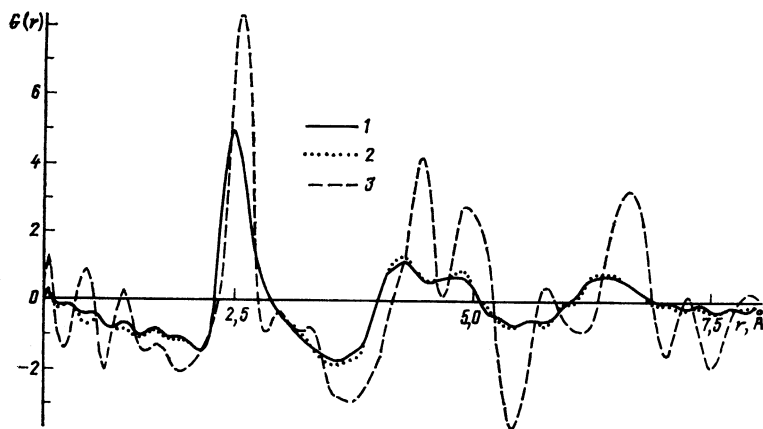


FIG. 8. Reduced radial distribution functions $G(r)$ of atoms in amorphous (1, 2) and crystalline (3) samples of PrNi_5 .

the absence of the gap and a finite value of the density of states beginning from zero energy, i.e., amorphization was accompanied by the appearance of low-energy states of the localized moment. The magnetic contribution to the entropy $S_M(T)$ at 50 K reached the value $R \ln 5$ in the crystalline state and $R \ln 3$ in the amorphous state (inset in Fig. 6a). Since the ground state of Pr^{3+} was a singlet in the ECF, the maximum "magnetic" entropy should be $R \ln 9$ [$R \ln(2J + 1)$], but this value was reached only at higher temperatures of the order of 300 K. The reduction in S_M (at 50 K) due to the amorphization indicated a shift of some of the states toward higher energies.

c. Determination of the radial distribution function

The room-temperature diffraction experiments were made by the time-of-flight method using a pulsed neutron source, which allowed the structure factor to be determined in a wide range of neutron momenta $0.5 < Q < 40 \text{ \AA}^{-1}$. When the structure factor was subjected to the Fourier transformation, the result was a reduced form of the radial distribution function of atoms $G(r)$ [see Eqs. (2)–(3)] with a resolution $\Delta r = 0.2 \text{ \AA}$ in the coordinate space.

Figure 7 gives the structure factors $S(Q)$ of two amorphous and crystalline samples of the compound PrNi_5 . In the case of the amorphous phase there was a small difference between the structure factors of the original amorphous and

annealed samples. The relative differences ($\sim \pm 2\text{--}3\%$) were half the experimental errors. The function $S(Q)$ obtained for the amorphous PrNi_5 had a clear precursor peak at $Q = 1.4 \text{ \AA}^{-1}$. This could be due to deviation of the atoms in the first and second coordination spheres from purely random packing.

Figure 8 shows the reduced radial distribution functions $G(r)$ of atoms in the amorphous and crystalline states. The functions were practically identical for the amorphous sample before annealing and after annealing up to 488 K. There were no significant differences either between $G(r)$ functions of two crystalline samples (samples Nos. 3 and 1.2.3). In view of the high resolution, the first coordination sphere of the amorphous sample included contributions of the partial Ni–Ni correlations in the form of the main peak at 2.5 Å and Ni–Pr in the form of a shoulder near 3 Å.

Figure 9 shows the functions $G(r)$ obtained for the amorphous samples of PrNi_5 and LaNi_5 (Ref. 12). They were clearly similar, indicating similarity of the structure parameters. A half-width at half-maximum of the first peak was of the order of 0.2 Å.

III. DISCUSSION OF RESULTS

It follows from the radial distribution functions of PrNi_5 that a number of conclusions can be drawn on the characteristics of the structure of the amorphous phase.

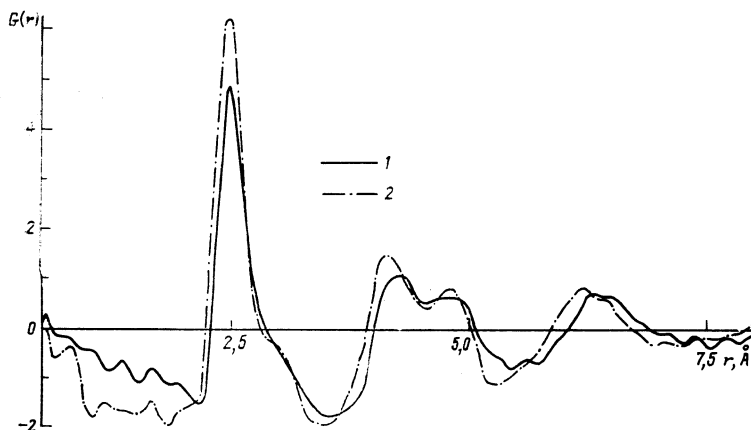


FIG. 9. Function $G(r)$ for amorphous PrNi_5 (1) and LaNi_5 (2) samples.¹²

There is great similarity, particularly in the first coordination spheres, between the structures of amorphous PrNi_5 and LaNi_5 , in particular, the widths (or the variances) of the distributions of the distances between the ions agreed with the error limits. The existence of a specific order, i.e., preference for the close neighborhood of Pr and Ni, could be assumed.

Separation of the partial contributions of the Ni–Ni and Ni–Pr correlations in the region of the first peak of $G(r)$ made it possible to estimate the shortest atomic distances in the amorphous system: $r_{\text{Ni-Ni}} = 2.50(2)$ Å and $r_{\text{Ni-Pr}} = 3.10(2)$ Å, which were close to the sums of the corresponding ionic radii ($R_{\text{Ni}} = 1.25$ Å and $R_{\text{Pr}} = 1.835$ Å). A comparison with the corresponding $G(r)$ function for the crystalline phase demonstrated that the average weighted distance between the first Ni–Pr neighbors in a crystal was considerably greater. The position of the first peak in the second coordination sphere was also shifted toward higher values of r . These results indicate that the packing was closer in the short-range atomic order of the amorphous system, i.e., that the microscopic (local) density of the amorphous samples was higher than in the crystalline state.

An analysis of the study of inelastic neutron scattering by PrNi_5 ($\text{Pr}_{16.7}\text{Ni}_{83.3}$) should answer two main questions: what is the origin of the magnetic scattering in the amorphous phase and what information on the structure of this phase can be obtained by analyzing the qualitative differences between the spectra of the amorphous and crystalline samples?

The experimental information on the nature of the magnetic scattering in the absence of a clear structure can be obtained from an analysis of the temperature dependence of the integral cross section in the $Q \rightarrow 0$ approximation.

In general, the total (integrated) cross section for the magnetic scattering of neutrons by rare-earth ions in the ECF (if the integration is carried out within the limits $-\infty < \hbar\omega < \infty$ and $T \gg \Delta_{CF}$, where Δ_{CF} is the scale of splitting by the ECF) must be a temperature-independent quantity corresponding to the value for a free ion:

$$\sigma_{\text{mag}}^{\text{tot}} = \sigma_{\text{mag}}^{\text{tot}}(\hbar\omega > 0) + \sigma_{\text{mag}}^{\text{tot}}(\hbar\omega \leq 0) = \frac{2}{3} \pi (g_N r_e)^2 g_J^2 J(J+1)$$

and equal to 7.74 b for Pr^{3+} . For the same reason it should be equal to the integrated cross section $\sigma_{\text{mag}}^{\text{tot}}(\hbar\omega > 0)$ at $T = 0$, i.e., when only the lowest state is populated. When temperature is increased, this cross section $\sigma_{\text{mag}}^{\text{tot}}(\hbar\omega > 0)$ should decrease because of a reduction in the contribution made by the excited states and, consequently, we should have $\sigma_{\text{mag}}^{\text{tot}}(\hbar\omega < 0) \neq 0$.

The temperature dependence of $\sigma_{\text{mag}}^{\text{tot}}(\hbar\omega > 0)$ is governed by the actual level-splitting scheme but in the case of stable rare-earth ions it should always be monotonically falling and should change significantly on the scale of $T \sim \Delta_{CF}$. Since a considerable contribution to the inelastic magnetic scattering in amorphous PrNi_5 comes from the region near the base of the elastic scattering line, it is necessary to separate the elastic components. The experimental results can be approximated most simply by two peaks with the Gaussian and Lorentzian profiles representing the narrow elastic peak and the wide inelastic scattering spectrum, respectively. When the area under the Lorentzian profile is integrated in

order to find $\sigma_{\text{mag}}^{\text{tot}}(\hbar\omega > 0)$, the “wings” are truncated at an energy of 50 meV (which leads to an error of $\sim 5\%$). In the case of a polycrystalline sample of PrNi_5 the value $\sigma_{\text{mag}}^{\text{tot}}(\hbar\omega > 0)$ is defined as the area under the peaks representing transitions between the ECF levels at different temperatures.

Figure 10 gives the temperature dependence of the total neutron scattering intensity in polycrystalline and amorphous samples accompanied by an energy loss $\sigma_{\text{mag}}^{\text{tot}}(\hbar\omega > 0)$. The experimental points are normalized by comparison with the calculated (using the energy level scheme of Ref. 9) intensities of the peaks of a polycrystalline sample at 4 and 13 meV.

At the lowest temperature it is found that $\sigma_{\text{mag}}^{\text{tot}}(\hbar\omega > 0)$ for the amorphous samples exceeds the corresponding value for crystalline PrNi_5 and the theoretical value for a free ion. This may be either due to an additional contribution of soft phonon modes or due to the influence of magnetic correlations between the Pr^{3+} ions (the molecular field constant for Pr^{3+} in crystalline PrNi_5 is nonzero). It is clear from Fig. 10 that the temperature dependence of the total scattering cross section of an amorphous sample resembles that of a polycrystalline sample, and their values are similar. We may therefore assume that the splitting of the ground multiplet of the Pr^{3+} ion in the inhomogeneous potential of the electric field does really exist in the amorphous phase. This is supported by the existence of the magnetic temperature-dependent contribution to the specific heat.

We can consequently relate the qualitative differences between the amorphous and crystalline samples, manifested by the magnetic inelastic neutron scattering and by the specific heat, to changes in the nature of splitting of the ground multiplet of Pr^{3+} as a result of amorphization. A possible reason for this change may be the appearance of a large number of inequivalent configurations of the immediate environment of the rare-earth ion.

To determine the main parameters of such a modification we use the model of randomization of the crystal field based on the averaging of the contributions made to the ECF potential by various possible configurations of the immediate environment of the rare-earth ion. The results of the cal-

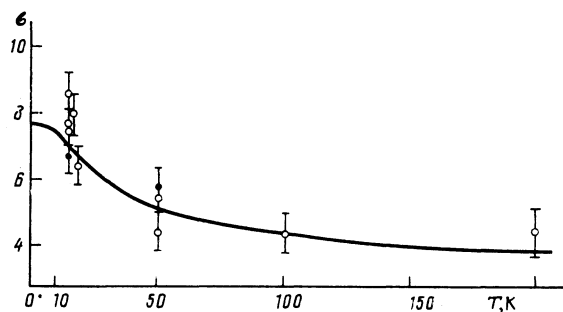


FIG. 10. Temperature dependence of the magnetic neutron scattering cross section $\sigma_{\text{mag}}^{\text{tot}}(\hbar\omega > 0)$ for the amorphous and crystalline states, plotted in the limit $Q \rightarrow 0$. The solid trace represents the value of $\sigma_{\text{mag}}^{\text{tot}}$ calculated for $\hbar\omega > 0$, starting from the energy level scheme of Pr^{3+} given in Ref. 9; (●) experimental values for a polycrystalline sample; (○) experimental values for amorphous samples.

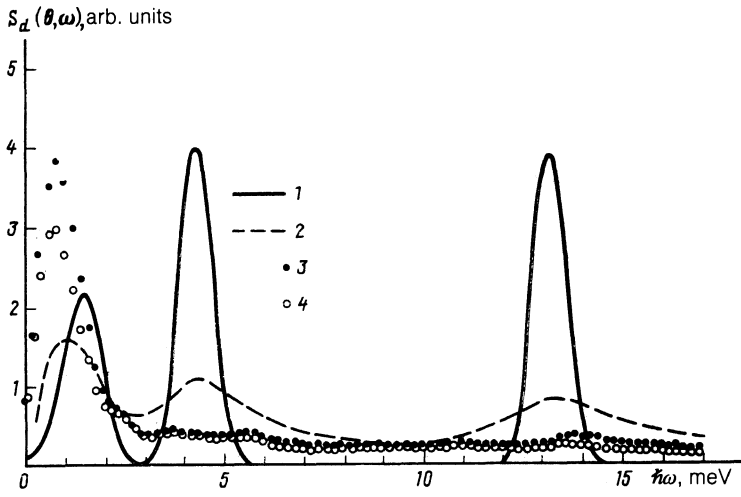


FIG. 11. Calculated spectra of $S_d(\theta, \omega)$ for the crystalline and amorphous states of PrNi_5 : 1) model spectrum of polycrystalline PrNi_5 at $T = 15$ K; the ECF parameters are taken from Ref. 9; 2) averaging of the model spectrum corresponding to the Hamiltonian (6) with the parameters taken from Ref. 9, which vary as a result of changes in their interatomic distances (see text) at $T = 15$ K; 3) results of averaging of the model spectrum calculated on the basis of variances of the parameters of the Hamiltonian (9), which allows for the orthorhombic distortions of the hexagonal symmetry at $T = 15$ K; 4) same as Fig. 3, but at $T = 50$ K.

calculations are presented in Fig. 11. In the first stage we average the spectra corresponding to the configurations differing in respect of the distance between the ions, but still retaining the hexagonal symmetry. We assume the Gaussian distribution of the distances between the ions with the full width at half-maximum amounting to 0.035 nm, which agrees with the scale of the distribution of the Pr–Ni distances estimated from the experimental function $G(r)$. A calculation of the energy level schemes for different configurations can be made by scaling up the experimental data for PrNi_5 (Ref. 9) using the relationships deduced from the model of effective point charges allowing for the presence of the 18 nearest nickel ions. Curves 1 and 2 in Fig. 11 represent the initial crystalline state and the spectra of PrNi_5 averaged in this way. Averaging over the distances smooths out the spectrum if there is no change in symmetry, but the result is still qualitatively different from the experimental data reported for the amorphous phase (Fig. 3) because of the presence of singularities (peaks) and the absence of a significant increase in the intensity in the limit $\hbar\omega \rightarrow 0$. These differences between the experimental and model spectra can be avoided if the calculations allow for lowering of the symmetry of the local environment of the rare-earth ion, but information about this aspect cannot be obtained directly from the diffraction data.

In the simplest case the Hamiltonian for a sample with a distortion of the symmetry can be represented as follows:

$$\hat{\mathcal{H}}_{\text{CEF}} = \hat{\mathcal{H}}_{\text{CEF}}^{\text{hex}} + B_2^2 \hat{O}_2^2. \quad (9)$$

The last term in Eq. (9) describes the influence of the orthorhombic distortion of the original hexagonal symmetry.²⁾

The lowering of the local symmetry completely lifts the degeneracy of the J multiplet and the wave functions of the levels change. In particular, the $\Gamma_4 - \Gamma_1$ transition from the ground state is now allowed and its probability rises rapidly as $|B_2^2|$ increases. If we limit $|B_2^2|$ to a value of the order of 0.5 meV, which corresponds to the scale of B_2^0 and may be represented geometrically as a change in the angular coordinates of the Ni–Pr bond by amounts within the limits of several degrees, it is found that the energy of this intense transition at low temperatures is basically within 1–2 meV. The total splitting of the multiplet then rises strongly. Aver-

aging over the scatter of the interionic distances and over this interval of B_2^2 gives the calculated curve 3, which describes quite well $S_d(\theta, \omega)$ of amorphous PrNi_5 . In view of the large statistical weight of the intense $\Gamma_4 - \Gamma_1$ transition characterized by a low energy, the intensity of neutron scattering rises near $\hbar\omega \approx 1$ meV, which changes to a fall at energies close to zero. It should be pointed out that heating produces the same changes in the calculated spectrum (curve 4) as found experimentally, i.e., the intensity falls in the range of low energy transfers. The proposed model predicts a reduction in the intensity of inelastic magnetic neutron scattering in the energy range < 1 meV, which can be checked experimentally using a spectrometer with a higher resolution.

It is interesting to analyze to what extent the proposed method for randomization of the crystal field makes it possible to describe the influence of amorphization on the magnetic component of the specific heat.

In the case of a polycrystalline sample we carried out calculations using Eq. (7) with the values of E_i given in Ref. 9. In an external magnetic field the energies of the ECF level are described by diagonalization of the Hamiltonian

$$\hat{\mathcal{H}}_{MC} = \hat{\mathcal{H}}_{\text{CEF}}^{\text{hex}} + g_J \mu_B (\mathbf{H}_e + \lambda \mathbf{M}) \cdot \mathbf{J}, \quad (10)$$

(the parameters B_n^m of PrNi_5 were taken from Ref. 9) subject to an additional self-consistency condition:

$$\mathbf{M} = -\mu_B g_J \langle \mathbf{J} \rangle, \quad (11)$$

where \mathbf{H}_e is the external field, $\lambda = \theta / C$ is the molecular field constant, θ is the paramagnetic temperature, C is the Curie constant of a free rare-earth ion, and \mathbf{M} is the magnetization per unit volume. The paramagnetic temperatures along different directions of an external magnetic field relative to the z axis are $\theta_{\perp} = 7$ K and $\theta_{\parallel} = 30$ K and are defined by fitting the calculated susceptibility PrNi_5 to the experimental data reported for a single crystal in Ref. 16.

The specific heat of a polycrystalline sample calculated allowing for the hexagonal symmetry of the lattice can be found from

$$\Delta C_M^{\text{pol}} = \frac{1}{3} (C_{\parallel} + 2C_{\perp}),$$

where C_{\perp} and C_{\parallel} are the specific heats calculated for an

external magnetic field perpendicular and parallel to the z axis. The results of these calculations with no field and in a field of 80 kG, made for a polycrystalline sample are plotted in Fig. 6a. We can see that the energy level scheme⁹ of Pr^{3+} allows us to reach a qualitative agreement between the experimental and calculated temperature dependences of the specific heat when an external field is applied; this supports the reliability of determination of not only the distribution of the levels, but also of their wave functions (this is true at least of the three or four lowest states).

In the case of an amorphous sample the diagonalization was carried out without the self-consistency procedure, since the molecular field constants were not known. The averaging was carried out allowing for the contribution made to ΔC_M and calculated for the same sets of the parameters B_n^m of the Hamiltonian

$$\hat{\mathcal{H}}_{MA} = \hat{\mathcal{H}}_{CEF}^{hex} + B_2^2 \hat{O}_2^2 + g_J \mu_B \mathbf{HJ}, \quad (12)$$

as had been used in modeling neutron spectra.

The relevant curves are plotted in Fig. 6b. Although the quantitative differences between the experimental and calculated curves are in this case larger than for a polycrystalline sample, it nevertheless follows that the simple model for the description of the ECF in amorphous PrNi_5 predicts correctly the main features of the behavior of ΔC_M of an amorphous sample: the weak temperature dependence in a wide range; the shift of the curve to the right (gap-formation effect) at low temperatures when the external field intensity is increased; the rise of ΔC_M with the field at temperatures in excess of 10 K. Consequently, the proposed approach to the description of the short-range order of amorphous RNi_5 (R is the rare-earth element) reflects the main differences between the crystalline and amorphous phases.

IV. CONCLUSIONS

We experimentally observed qualitative differences in the spectra of magnetic and elastic neutron scattering, and in the temperature and magnetic-field dependences of the specific heat between amorphous and crystalline phases of PrNi_5 . The influence of amorphization on the spectrum of magnetic excitations cannot be regarded simply as broadening of the peaks responsible for the well-defined transitions between the levels of the Pr^{3+} ion in the ECF, which were well known for the crystalline phase. Experimentally, in addition to an annihilation of these strong peaks, a considerable increase in the intensity of the spectrum was observed at low transferred energies ($\hbar\omega \leq 2$ meV). The presence of a definite distribution of the density of magnetic states at low energies demonstrates that the temperature dependence of the magnetic contribution to the specific heat of $\text{Pr}_{16.7}\text{Ni}_{83.3}$ is transformed strongly when an external magnetic field is applied.

The nature of the influence of amorphization on the ECF effects, which reflects essentially the characteristics of the structure on the atomic scale, was explained by developing a model of a deformed crystal. Within the framework of this model we allowed for changes in the atomic distances and for distortions of the local symmetry of the distances and for distortions of the local symmetry of the distribution of ions as a result of amorphization. The neutron spectra and the magnetic contribution to the specific heat calculated on

the basis of the simplest assumptions made it possible to reproduce the main outlines of the observed dependences, i.e., the selected model does indeed reflect the fundamental differences of the real structure of amorphous RNi_5 intermetallics from their crystalline analogs.

Moreover, we established the following.

1. No significant effects of structural relaxation in the amorphous phase are manifested on the scale of the interatomic distances. The transition from the amorphous to the crystalline state, at least where the local topology is involved, occurs in a fairly narrow range of temperatures on the order of a few percent of the crystallization temperature.

2. The shortest distances between the nickel and praseodymium ions in the amorphous state are somewhat less than in the crystalline phase. The smaller interionic distances, compared with the equilibrium values, are observed also in the crystalline phase immediately after crystallization. This is followed by relaxation as the annealing temperature is increased.

The proposed approach and the results obtained can be used in an analysis of magnetic properties of the investigated compounds and in the development of microscopic models of the real structure of amorphous alloys.

The authors are deeply grateful to S. L. Isakov, V. V. Kotupov, N. M. Parovik, S. A. Tereshchenko, A. S. Ivanov, and E. S. Klement'ev for their help in the experiments, and to the Laue-Langevin Institute for kindly providing an opportunity to carry out measurements using the IN-4 spectrometer.

¹ Institut für Nukleare Festkörperphysik, Kernforschungszentrum Karlsruhe, Germany.

² More detailed calculations including B_4^2 and B_6^2 show that these coefficients cannot be regarded as making negligible contributions compared with B_2^2 . However, their effects tend to cancel and the results of complete calculations after the averaging procedure are close to the results obtained allowing for B_2^2 alone.

³ S. Steeb and P. Lamparter, *J. Non-Cryst. Solids* **61-62**, 237 (1984).

⁴ E. Svab and S. N. Ishmaev, *Proc. Fifth Intern. School on Neutron Physics*, Alushta, USSR, 1987, p. 287.

⁵ P. Fulde and M. Lowenhaupt, *Adv. Phys.* **34**, 589 (1985).

⁶ J.-C. Ousset, S. Cantaloup, J. Durand, and D. Bertrand, *J. Non-Cryst. Solids* **61-62**, 385 (1984).

⁷ W. Felsch and H. Schröder, *Solid State Commun.* **45**, 1043 (1983).

⁸ Y. Nishihara, T. Katayama, and S. Ogawa, *J. Phys. Soc. Jpn.* **51**, 2487 (1982).

⁹ B. D. Rainford, V. Samadian, R. J. Begum *et al.*, *J. Appl. Phys.* **53**, 7725 (1982).

¹⁰ P. A. Alekseev, O. K. Alekseeva, V. N. Lazukov *et al.*, *Fiz. Khim. Obrab. Mater.* No. 1, 63 (1989).

¹¹ P. A. Alekseev, I. P. Sadikov, A. Andreeff, H. Griessmann *et al.*, *Phys. Status Solidi B* **97**, 87 (1980).

¹² S. L. Isakov and S. N. Ishmaev, Preprint No. IAÉ-4654/9 [in Russian], Institute of Atomic Energy, Moscow (1988).

¹³ P. A. Alekseev, V. N. Lazukov, A. Yu. Rumyantsev, and I. P. Sadikov, *J. Magn. Magn. Mater.* **75**, 323 (1988).

¹⁴ S. L. Isakov, S. N. Ishmaev, P. A. Alekseev *et al.*, *Fiz. Tverd. Tela (Leningrad)* **28**, 1240 (1986) [*Sov. Phys. Solid State* **28**, 699 (1986)].

¹⁵ A. N. Kolmogorov, *Izv. Akad. Nauk SSSR Otd. Mat. Estestv. Nauk Ser. Fiz.* **3**, 335 (1937).

¹⁶ M. N. Khlopkin, N. A. Chernoplekov, and P. A. Chermnykh, Preprint No. IAÉ-3549/10 [in Russian], Institute of Atomic Energy, Moscow (1982).

¹⁷ G. Kh. Panova, N. A. Chernoplekov, A. A. Shikov *et al.*, *Zh. Eksp. Teor. Fiz.* **88**, 1012 (1985) [*Sov. Phys. JETP* **61**, 595 (1985)].

¹⁸ K. Andres, S. Darack, and H. R. Ott, *Phys. Rev. B* **19**, 5475 (1979).

Translated by A. Tybulewicz